The quasar main sequence and its potential for cosmology

**Paola Marziani[1], Deborah Dultzin[2], Ascensión del Olmo[3]†,
Mauro D'Onofrio[4], José A. de Diego[2], Giovanna M. Stirpe[5],
Edi Bon[6], Natasa Bon[6], Bożena Czerny[7], Jaime Perea[3],
Swayamtrupta Panda[7,8], Mary Loli Martinez-Aldama[3,7]
and C. A. Negrete[2]**

[1]INAF, Osservatorio Astronomico di Padova, Italy
email: paola.marziani@inaf.it

[2]Instituto de Astronomía, UNAM, Mexico

[3]IAA (CSIC), Granada, Spain

[4]Università di Padova, Italy

[5]INAF, OASS, Bologna, Italy

[6]Belgrade Observatory, Serbia

[7]Center For Theoretical Physics, Polish Academy of Sciences, Warsaw, Poland

[8]Nicolaus Copernicus Astronomical Center, Polish Academy of Sciences, Warsaw, Poland

Abstract. The main sequence offers a method for the systematization of quasar spectral properties. Extreme FeII emitters (or extreme Population A, xA) are believed to be sources accreting matter at very high rates. They are easily identifiable along the quasar main sequence, in large spectroscopic surveys over a broad redshift range. The very high accretion rate makes it possible that massive black holes hosted in xA quasars radiate at a stable, extreme luminosity-to-mass ratio. After reviewing the basic interpretation of the main sequence, we report on the possibility of identifying virial broadening estimators from low-ionization line widths, and provide evidence of the conceptual validity of redshift-independent luminosities based on virial broadening for a known luminosity-to-mass ratio.

Keywords. quasars: general, quasars: emission lines, line: profiles, cosmological parameters, distance scale, dark matter

1. Introduction

The concept of the quasar main sequence originated from a Principal Component Analysis of parameters measured on the optical spectra of $\sim$80 PG quasars (Boroson & Green 1992). The first eigenvector 1 (E1) computed by the analysis was found to be mainly associated with two anti-correlations, between strength of FeIIλ4570 and prominence of [OIII]$\lambda\lambda$4959, 5007, and strength of FeIIλ4570 and FWHM of the HI Balmer line Hβ. In the plane FWHM Hβ vs. prominence of the optical FeII emission (where the FeII prominence is measured by the parameter R_{FeII} defined as the intensity ratio of the FeII λ4570 blend and Hβ), the occupation of data points representing low redshift quasars takes the form of an elbow-shaped sequence (Fig. 1). Quasar spectra show a wide range of line widths, profile shapes, R_{FeII}, line shifts, line intensities which imply differences in
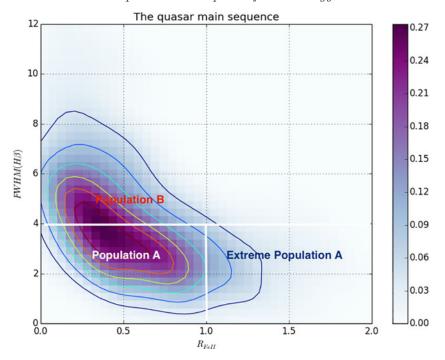
Figure 1. The optical plane of the E1 MS, FWHM of the broad component of Hβ vs R_{FeII}. Isodensity curves and shading represent the source occupation from the sample of Zamfir *et al.* (2010), with ≈ 300 quasars. The labels identify the loci of the main populations: Population A with FWHM $\leqslant 4000$ km s^{-1}; Population B with FWHM > 4000 km s^{-1}; extreme Population A, $R_{\mathrm{FeII}} > 1$. See text for more details.

line emitting gas dynamics and ionization levels: the main sequence organizes different properties (Sulentic *et al.* 2000).

Why are these two parameters – FWHM Hβ and R_{FeII} – so important? FeII emission extends from UV to the IR and can dominate the thermal balance of the low-ionization part of the broad-line region (BLR, Marinello *et al.* 2016). FeII emission is self-similar (at least to a first approximation) in quasars but FeII intensity with respect to Hβ changes from object to object. The FWHM(Hβ) is explained mainly by Doppler broadening, and is related to projection of the velocity field in the low-ionization BLR along the line of sight. There has been a growing consensus that the low-ionization BLR is predominantly virialized, since the early results of the first major reverberation mapping campaigns (Peterson & Wandel 1999). Therefore R_{FeII} and FWHM Hβ can be considered tracers of the physical and dynamical conditions in the low-ionization BLR. Sulentic *et al.* (2000) introduced the distinction between two Populations. The FWHM H$\beta \leqslant 4000$ km s^{-1} condition selects narrower sources that are preferentially moderate-to-strong FeII emitters (Population A). Broader sources (FWHM H$\beta > 4000$ km s^{-1}, Population B) tend to have low FeII emission and are believed to be *predominantly* sources radiating at lower Eddington ratio (L/L_{Edd}) than the quasars of Population A (Marziani *et al.* 2018a).

2. The main driver of the quasar main sequence

Several approaches consistently support a relation between Eddington ratio and R_{FeII}. For instance, according to the fundamental plane of accreting massive black holes for reverberation-mapped active galactic nuclei (AGNs) – a relation connecting R_{FeII}, L/L_{Edd} and a parameter D dependent on line shape (Du *et al.* 2016) – $R_{\mathrm{FeII}} > 1$ implies

$L/L_{\text{Edd}} > 1$. An independent confirmation is provided by the analysis of the stellar velocity dispersion of the host spheroid, $\sigma_\star$. The $\sigma_\star$ has been used as a proxy for the black hole mass in accordance with established scaling laws connecting black hole and host spheroid mass (e.g., Magorrian *et al.* 1998). If the AGNs are subdivided in narrow luminosity bins, the $\sigma_\star$ is found to decrease as a function of R_{FeII}, implying that R_{FeII} increases as a function of L/L_{Edd} (Sun & Shen 2015). The origin of this connection remains unclear at the time of writing. The structure of the emitting regions is probably influenced by the balance between gravitation and radiation forces (Ferland *et al.* 2009), and by a change in accretion mode with increasing L/L_{Edd} (Wang *et al.* 2014). So the correlation may be a secondary effect of structural changes induced on the BLR (Panda *et al.* 2019). Since R_{FeII} is also dependent on metallicity (Panda *et al.* 2018), high L/L_{Edd} might be associated with enriched gas provided to the emitting region by nuclear and circumnuclear star formation (D'Onofrio & Marziani 2018).

Outflows from mildly-ionized gases producing blue shifted lines from ionic species of IP $\lesssim 50$ eV are ubiquitous in AGNs (Richards *et al.* 2011). The extent and the energetics of the outflows are not yet fully appreciated. For example, it has been possible only in recent year to consider high velocity outflows from very hot gas (the so-called ultra-fast outflows, UFOs, Tombesi *et al.* 2011). However, the prominence of outflows traced by the mildly-ionized gas emitting CIVλ1549 and [OIII]$\lambda\lambda$4959,5007 increases along the main sequence (MS, see Figure 4 of Sulentic *et al.* 2000 for CIV) and reaches a maximum in correspondence of the strongest FeII emitters, at extreme values of L/L_{Edd}.

Several interpretations of the MS (not necessarily in contradiction among themselves) have been proposed. The occupation of data points can be accounted for by a trend between Eddington ratio and R_{FeII}, convolved with the effect of orientation on the FWHM of Hβ (Marziani *et al.* 2001; Shen & Ho 2014). This is especially true in the case of a small range of black hole masses. There is a degeneracy between the effect of black hole mass and orientation as both tend to increase the FWHM of Hβ (Marziani *et al.* 2018a). Panda *et al.* (2019) showed that, for a fixed black hole mass, there is a limit in FWHM beyond which the orientation effects cannot go. Even if limits to the FWHM range spanned by orientation broadening can be set, the overlap of mass and orientation effects implies that, in the 2D representation of the MS, it is impossible to independently retrieve these parameters (viewing angle, L/L_{Edd}, black hole mass) for individual quasars. A 3D representation of the MS or additional constraints are necessary. Another important side effect of the degeneracy between mass and viewing angle is that a broad range of black hole mass leads to the MS with a wedge-shaped occupation area (Shen & Ho 2014).

An alternative view considers that Population B quasars are more massive and radiate at lower values of the L/L_{Edd} than quasars belonging to Population A. This difference between the two populations helps define the shape of the main sequence *as a sequence* in the optical plane, and is most likely a consequence of the down-sizing of nuclear activity at low redshift (Fraix-Burnet *et al.* 2017). So it is possible to establish an evolutionary connection from the sources of extreme Population A to the ones of Population B, where the cosmic arrow of time is provided by the black hole mass which can only grow: the larger the mass the older the source.

3. Highly-accreting quasars

Extreme Population A (xA) quasars satisfy the condition $R_{\text{FeII}} > 1$; they are those $\sim 10\%$ of quasars in low-z ($\lesssim 1$), optically selected samples with extreme FeII emission. Their prevalence is steeply decreasing toward higher R_{FeII} values: in the range $1.0 \leqslant R_{\text{FeII}} < 1.5$ we find ≈ 7 % of all quasars; in the range $1.5 \leqslant R_{\text{FeII}} < 2, \approx 3$ %. Quasars with $R_{\text{FeII}} > 2$ account for less than 1% of the optically-selected quasar population (Marziani *et al.* 2013). xA quasars show distinctive features: their UV continuum is usually

not reddened, they are often with extremely weak UV emission lines (i.e., weak-lined quasars with W(CIV)λ1549 $\leqslant$ 10Å following Diamond-Stanic *et al.* 2009). The prominent AlIIIλ1860, and very weak CIII]λ1909 allow for easy UV selection criteria: if (1) $R_{\mathrm{FeII}} >$ 1.0 is satisfied, then (2) UV AlIII λ1860/SiIII]λ1892 > 0.5 & SiIII]λ1892/CIII]λ1909 > 1.

Physical parameters are correspondingly extreme. First of all, their L/L_{Edd} is at the high end of the distribution along the main sequence, with small dispersion (Marziani & Sulentic 2014). In other words xA quasars selected according to criteria 1 and 2 are extreme radiators, with maximum radiative output per unit mass close to their Eddington limit. This condition is predicted by accretion disk theory at high (possibly super-Eddington) accretion rates: radiative efficiency should be low, and L/L_{Edd} saturate toward a limiting value (Sadowski *et al.* 2014, and references therein). The star formation rate (SFR) in the host galaxy as estimated from radio observations can be up to $\sim$ a few $10^3 \mathrm{M}_\odot$ yr^{-1} (Ganci *et al.* 2019, $z \lesssim 1$). The broad emission line intensity ratios in the UV suggest extremely high values for density ($n \gtrsim 10^{12} - 10^{13}$ cm^{-3}), very low ionization (ionization parameter $\sim 10^{-3} - 10^{-2.5}$, Negrete *et al.* 2012), and high metallicity ($Z \gtrsim 20$ Z$_\odot$, Martínez-Aldama *et al.* 2018).

Broad emission lines in xA sources are produced by gas apparently enriched by a circumnuclear Starburst. It is tempting to consider that xAs could be the first unobscured stage emerging from obscured stages of AGN evolution. This hypothesis fits an evolutionary sequence (Sanders *et al.* 1988; Dultzin-Hacyan *et al.* 2003): merging and strong interaction lead to accumulation of gas in the galaxy central parsecs, and to coeval Starburst and nuclear activity, whereas winds from massive stars and supernovæ provide enriched material. Feedback effects on the host galaxies induced by the extreme outflows of xA quasars can be significant if the AGN luminosity is high, as the outflow thrust and kinetic powers are dependent on the emission line luminosity. This means that xA quasars could likely be a major factor in galactic evolution at moderate-to-high redshift ($z \gtrsim 1$). It is however important to stress that xA sources are not necessarily luminous sources – xAs are the low-mass (relatively rare) high accretors in the local Universe as well as the most distant quasars at $z \gtrsim 6$ (Wang *et al.* 2019).

Almost symmetric Hβ and AlIIIλ1860 line profiles coexist with a CIVλ1549 profile shifted by several thousand km/s, even at the highest luminosity and when radiation forces predominate over gravity, i.e., when L/L_{Edd} is high (Sulentic *et al.* 2017; Vietri *et al.* 2018; Bischetti *et al.* 2017). A virialized subsystem emitting low ionization lines and a subsystem due to winds or outflows constitute two regions that are, at least in part, appearing as kinematically disjoint in the line profiles.

In addition, we can count on xA quasars' spectral invariance: intensity ratios remain the same; only the line width increases with luminosity. This implies that the radius of the emitting region should rigorously scale as $L^{\frac{1}{2}}$: if not, the ionization parameter should change with luminosity. No significant spectral change from very high luminosity to low luminosity sources has been detected yet. Putting together (1) $L/L_{\mathrm{Edd}} = const.$, (2) $r \propto L^{\frac{1}{2}}$ and the virial condition (3) $M_{\mathrm{BH}} \propto r$FWHM^2, we obtain a relation linking luminosity and line width as $L \propto$ FWHM^4 (Marziani & Sulentic 2014).

Building the Hubble diagram distance modulus versus redshift (see e.g., Risaliti & Lusso 2015) from the redshift-independent virial luminosity estimates with xA quasars over the redshift range $0.1 \lesssim z \lesssim 3$, we obtain a distribution consistent with concordance ΛCDM (Fig. 2). Constraints on the energy density of matter Ω_{M} (0.30 ± 0.06) are better than the ones from supernovæ, because of the $z \sim 2$ coverage of the quasar sample. The significant scatter of individual measurements ($\sim 1.1 - 1.3$ mag) may be associated with (a) uncertainty of FWHM, which enters with the 4th power in the luminosity relation; (b) orientation that is likely to be the main source of scatter in the classical scaling
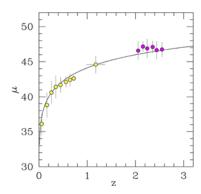
Figure 2. The Hubble diagram distance modulus μ vs z for a sample of quasars (Dultzin *et al.* 2020). Individual measurements have been averaged over redshift bins. Error bars are sample standard deviations for z and μ. Yellow data point refer to the use of the Hβ FWHM as a virial broadening estimator, magenta ones are computed from the FWHM of the AlIIIλ1860 doublet individual components. Error bars show sample standard deviations in μ and z for each bin.

relations (Marziani *et al.* 2019); (c) differences in intrinsic properties of the xA quasars i.e., spectral energy distribution, ionizing photon flux, etc.

4. Conclusion

The MS offer contextualization of quasar observational and physical properties (Marziani *et al.* 2018b). Several MS trends are ultimately associated with Eddington ratio which apparently reaches an extreme value in correspondence of the extreme Population A (xA). xA quasars include the strongest FeII emitters, satisfying the condition $R_{\mathrm{FeII}} > 1$. They show a relatively high prevalence (10%) and are easily recognizable thanks to their peculiar and luminosity-invariant spectral properties. In addition, they are sources that tend to show low intrinsic variability (Du *et al.* 2018), and their low ionization lines are apparently emitted in a virialized BLR (see also Swayamtrupta Panda's contributions in this volume). These properties make xA quasars suitable as possible *Eddington* standard candles, where the invariant properties is not intrinsic luminosity, but Eddington ratio.

References

Bischetti, M., Piconcelli, E., Vietri, G., *et al.* 2017, *AAp*, 598, A122
Boroson T. A. & Green R. F. 1992, *ApJS*, 80, 109
Diamond-Stanic, A. M., Fan, X., Brandt, W. N., *et al.* 2009, *ApJ*, 699, 782
D'Onofrio, M. & Marziani, P. 2018, *FrASS*, 5, 31
Du, P., Zhang, Z.-X., Wang, K., *et al.* 2018, *ApJ*, 856, 6
Du, P., Wang, J.-M., Hu, C., *et al.* 2016, *ApJL*, 818, L14
Dultzin, D., Marziani, P., de Diego, J. A., Negrete, C. A., *et al.* 2020, *FrASS*, 6, 80
Dultzin-Hacyan, D., Krongold, Y., & Marziani, P. 2003, *RMexAAp CS*, 79
Ferland, G. J., Hu, C., Wang, J.-M., *et al.* 2009, *ApJL*, 707, L82
Fraix-Burnet, D., D'Onofrio, M., & Marziani, P. 2017, *FrASS*, 4, 20
Ganci, V., Marziani, P., D'Onofrio, M., *et al.* 2019, *A&A*, 630, A110
Magorrian, J., Tremaine, S., Richstone, D., *et al.* 1998, *AJ*, 115, 2285
Marinello, M., Rodríguez-Ardila, A., Garcia-Rissmann, A., *et al.* 2016, *ApJ*, 820, 116
Martínez-Aldama, M. L., del Olmo, A., Marziani, P., *et al.* 2018, *AAp*, 618, A179
Marziani, P., Sulentic, J. W., Plauchu-Frayn, I., del Olmo, A., *et al.* 2013, *A&A*, 555, 89
Marziani, P., Sulentic, J. W., Zwitter, T., *et al.* 2001, *ApJ*, 558, 553
Marziani, P., del Olmo, A., D'Onofrio, M., *et al.* 2018a, PoS, 328, 2
Marziani, P., Dultzin, D., Sulentic. J, W., Del Olmo, A., *et al.* 2018b, *FrASS*, 5, 6

Marziani, P., del Olmo, A., Martínez-Carballo, M. A., *et al.* 2019, *AAp*, 627, A88

Marziani, P. & Sulentic, J. W. 2014, *MNRAS*, 442, 1211

Negrete, C. A., Dultzin, D., Marziani, P., *et al.* 2012, *ApJ*, 757, 62

Negrete, C. A., Dultzin, D., Marziani, P., *et al.* 2018, *AAp*, 620, A118

Panda, S., Czerny, B., Adhikari, T. P., *et al.* 2018, *ApJ*, 866, 115

Panda, S., Marziani, P., & Czerny, B. 2019, *ApJ*, 882, 79

Peterson, B. M. and Wandel, A. 1999, *ApJL*, 521, L95

Richards, G. T., Kruczek, N. E., Gallagher, S. C., *et al.* 2011, *AJ*, 141, 167

Risaliti, G. & Lusso, E. 2015, *ApJ*, 815, 33

Sadowski, A., Narayan, R., McKinney, J. C., *et al.* 2014, *MNRAS*, 439, 503

Sanders, D. B., Soifer, B. T., Elias, J. H., *et al.* 1988, *ApJL*, 328, L35

Shen, Y. & Ho, L. C. 2014, *Nature*, 513, 210

Sulentic, J. W., del Olmo, A., Marziani, P., *et al.* 2017, *AAp*, 608, A122

Sulentic, J. W., Marziani, P., & Dultzin-Hacyan, D. 2000, *ARAAp*, 38, 521

Sulentic, J. W., Zwitter, T., Marziani, P., *et al.* 2000, *ApJL*, 536, L5

Sun, J. & Shen, Y. 2015, *ApJL*, 804, L15

Tombesi, F., Cappi, M., Reeves, J. N., *et al.* 2011, *ApJ*, 742, 44

Vietri, G., Piconcelli, E., Bischetti, M., *et al.* 2018, *AAp*, 617, A81

Wang, F., Yang, J., Fan, X., *et al.* 2019, *ApJ*, 884, 30

Wang, J.-M., Qiu, J., Du, P., *et al.* 2014, *ApJ*, 797, 65

Zamfir, S., Sulentic, J. W., Marziani, P., *et al.* 2010, *MNRAS*, 403, 1759